A Solution for Ice Accretion Detection on Wind Turbine Blades

Jocelyn Sabatier[1], Patrick Lanusse[2], Benjamim Feytout[3] and Serge Gracia[3]
[1]*Bordeaux University, IMS Lab., UMR 5218 CNRS, 351 Cours de la Libération, 33405 Talence, France*
[2]*Bordeaux INP, IMS Lab., UMR 5218 CNRS, 351 Cours de la Libération, 33405 Talence, France*
[3]*VALEOL, Parc de l'Intelligence Environnementale, 213 Cours Victor Hugo, 33323 Bègles Cedex, France*

Keywords: Wind Turbine, Blade Ice Detection, Observer, Anti-icing Device.

Abstract: This paper proposes a solution for ice accretion detection on wind turbine blades. The solution involves an active deicing device that uses a conductive polymer paint to heat relevant surfaces of the blade under electric potential difference. This deicing system is used here to perform a dynamic thermal characterization of the blade for various operating conditions (with or without ice, with or without wind). The dynamical behavior differences highlighted are then exploited using a dynamic observer to detect ice accretion through the control signal produced by the observer. Tests carried out in a climatic chamber showed the validity and the accuracy of the proposed method.

1 INTRODUCTION

Cold areas are often attractive regions for wind turbine installation for two main reasons:

- they are well exposed to wind,
- the low temperatures increase air density, thus increasing the kinetic energy of the wind and consequently, the power captured by the wind turbine.

However, their wind turbine blades are subjected to icing which can lead to serious consequences for the production, maintenance and durability of the whole turbine (Jasinski *et al.*, 1998) (Hochart *et al.*, 2008).

Ice accretion can be caused by freezing rain, drizzle, freezing fog, or frost when the wind turbine is installed near water bodies. It usually appears on the intrados (to a lesser degree) and extrados, and / or on the leading and trailing edges (Kraj and Bibeau, 2010).

Icing reduces the aerodynamic efficiency of the blades as it changes the blade geometrical profile. This leads to production losses (Jasinski *et al*., 1998), (Ronsten, 2004).

Ice accretion also creates additional and unbalanced loads that cause increased material fatigue, leading to premature wear or damage to major elements of the kinematic chain (impact on the multiplier and the generator) (Ganander and Ronsten, 2003) (Frohboese and Anders, 2007) (Virk *et al*., 2010). The mass of accumulated ice can significantly increase vibrations and also the radial loads on the blades due to centrifugal force. The system fastening the blades to the hub must be specifically sized to support the extra stress and avoid mechanical failure. Such a situation may require stopping the turbine during severe frost events.

From a safety point of view, chunks of ice can be detached during the turbine shutdown or can be projected during operation, causing lethal risks to maintenance operators or any other person in the vicinity of the wind turbine (Seifert, 2003).

Many solutions have been proposed in the literature to fight against turbine blade ice accretion (Parent and Ilinca, 2011), such as passive technologies, which aim to prevent the formation of ice on the blades (Kimura *et al*., 2003), (Dalili *et al*., 2009), or active technologies which operate when ice is detected. Most of these technologies come from the field of aviation and are based on mechanical deformation or the use of a heater for the leading edge (Botura and Fisher 2003) (Laakso and Peltola, 2005).

Active technologies require a means to detect ice accretion. According to (Homola *et al.*, 2006) and (Parent and Ilinca, 2011), icing can be detected either directly or indirectly. Direct methods detect a change in a physical property caused by ice

Sabatier, J., Lanusse, P., Feytout, B. and Gracia, S.
A Solution for Ice Accretion Detection on Wind Turbine Blades.
DOI: 10.5220/0006403904140421
In *Proceedings of the 14th International Conference on Informatics in Control, Automation and Robotics (ICINCO 2017) - Volume 1*, pages 414-421
ISBN: 978-989-758-263-9

accretion such as (and not cited in (Homola *et al.*, 2006) (Parent and Ilinca, 2011)) mass (Skrimpas *et al.*, 2016), reflective properties (Berbyuk *et al.*, 2014), electrical or thermal conductivity, dielectric coefficient and inductance (Owusu *et al.*, 2013). Indirect methods are based upon detecting the weather conditions that lead to icing (humidity and temperature).

In this paper, a direct method is proposed. It involves a de-icing device built by the authors and recently published (Sabatier *et al.*, 2016). This de-icing device uses a conductive polymer paint to heat relevant surfaces of the blade under potential difference. It is used here to perform a dynamical thermal characterization of the blade for various operating conditions (with or without ice, with or without wind). The dynamical behavior differences highlighted are then exploited using a dynamic observer to detect ice accretion through the control signal produced by the observer.

2 PROTOTYPE AND DEICING DEVICE PRESENTATION

The proposed ice accretion detection method involves an active de-icing device recently published (Sabatier *et al.*, 2016). This de-icing device is based on heating relevant surfaces of the blade with conductive polymer paint under electric potential difference (Rescoll, 2011). Current flow through the paint film causes heating by the Joule effect that is proportional, among other things, to the film surface and thickness. The paint strip power supply is ensured by electrodes connected to the wind turbine auxiliaries from the hub.

For dynamical modeling and to evaluate the ice accretion detection method, prototypes of the blade root and the blade tip were constructed (figure 1). They integrate different layers of paint (grey parts) and thermocouples. They were used in a climatic wind tunnel at the “Centre Scientifique et Technique du Bâtiment (CSTB)” in Nantes (France) to learn more about how frost develops on a blade and especially on what parts of the blade. These prototypes were also used to obtain a dynamical model linking the voltage applied on the blade to the temperature at various points of the paint strips and also to validate the temperature control system.

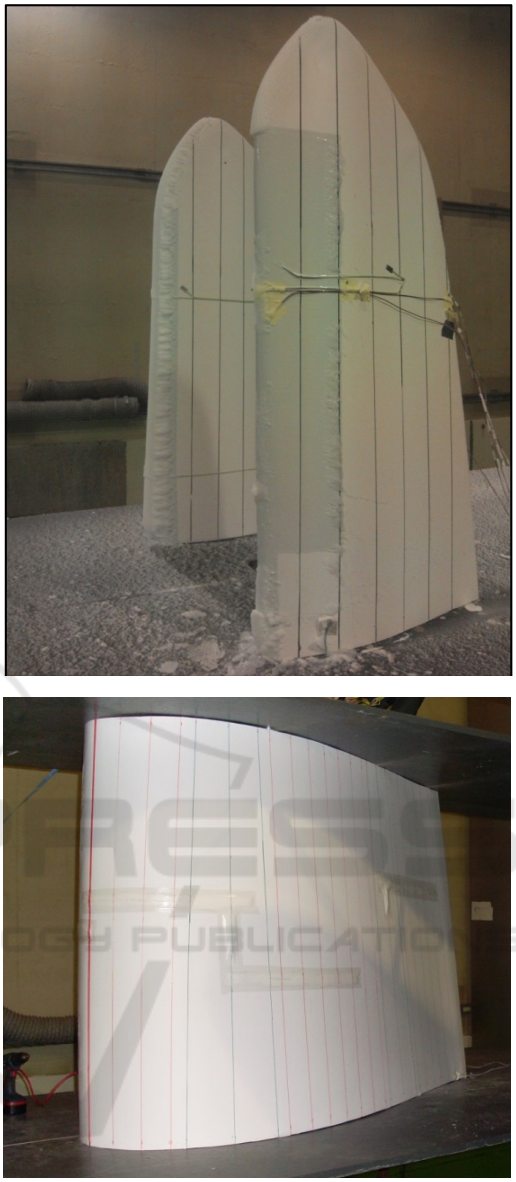

Figure 1: Blade tip and blade root prototypes used in the atmospheric wind tunnel.

3 THERMAL MODELING

3.1 Thermal Model with or without Ice

To obtain a thermal model of the blade heating system, the simplified representation of figure 2 was used. It comprises a blade (fiberglass and epoxy resin) having a large size (in the longitudinal direction, not shown here) fitted with two electrodes and then partially covered with paint. A sensor measures the temperature at the center of the paint

strip. The assembly is protected and separated from ambient air by a layer of gelcoat.

As shown in (Sabatier *et al.*, 2016), the thermal resistance and capacity of the blade (epoxy resin) can be neglected due to the high thermal resistance value of the blade. **Without ice**, the resulting thermal model is thus represented by figure 3, where T_{paint} and T_{amb} are respectively the paint & gelcoat temperature and the ambient air temperature. R_{paint} and C_{paint} are respectively the thermal resistance and capacity of the paint & gelcoat. P_{elec} is the thermal power produced by the paint and h is the paint-air convection coefficient. In view of the low respective thicknesses of the paint and the gelcoat, they were considered as the same material.

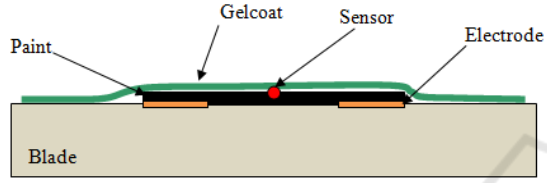

Figure 2: Simplified representation (transverse section) of the blade, the conductive paint, the electrode and the gelcoat protection.

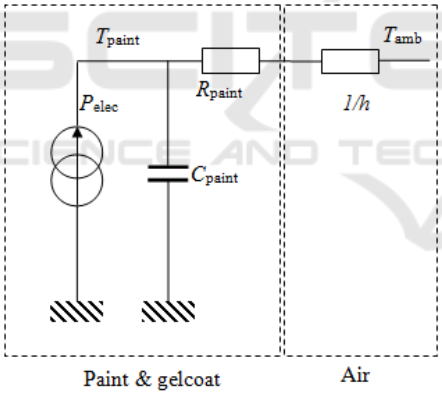

Figure 3: Simplified thermal model without ice.

From figure 3 and in the Laplace domain, the following equation linking the temperature of the paint to the electrical power and the ambient temperature can be obtained:

$$T_{paint}(s) = \frac{1}{1+\frac{s}{\omega_c}}\left(\frac{K}{\omega_c}P_{elec}(s)+T_{amb}(s)\right) \quad (1)$$

with:

$$\omega_c = \frac{1}{(R_{paint}+1/h)C_{paint}} \quad \text{and} \quad K = \frac{1}{C_{paint}}. \quad (2)$$

With ice, an RC cell representing the ice layer must be added between the paint & gelcoat and ambient air, as shown by figure 4, where R_{ice} and C_{ice} are respectively the thermal resistances and capacities of the ice.

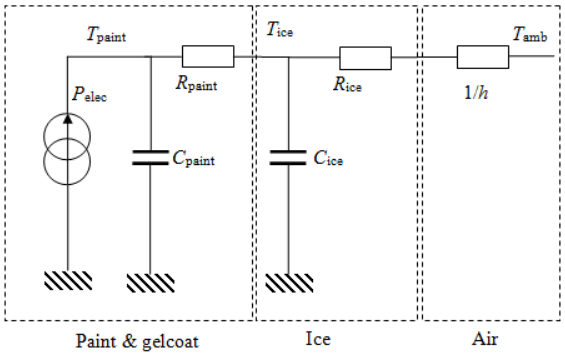

Figure 4: Thermal model with ice.

From the model in figure 4, it can be shown that:

$$T_{paint}(s)\left(sC_{paint}+\frac{1}{R_{paint}}\right) = P_{elec}(s)+\frac{T_{ice}(s)}{R_{paint}} \quad (2)$$

and

$$T_{ice}(s) = \frac{\frac{T_{paint}(s)}{R_{paint}}+\frac{T_{amb}(s)}{R_{ice}+1/h}}{sC_{ice}+\frac{1}{R_{paint}}+\frac{1}{R_{ice}+1/h}}$$

or after simplification

$$T_{paint}(s) = K_1\frac{1+\frac{s}{\omega_1}}{1+\frac{2z}{\omega_2}s+\left(\frac{s}{\omega_2}\right)^2}\left(P_{elec}(s)+\frac{K_2}{1+\frac{s}{\omega_3}}T_{amb}(s)\right) \quad (3)$$

with

$$K_1 = R_{paint}+R_{ice}+1/h\,,\ \omega_1 = \frac{{R_{paint}}^2 C_{ice}}{R_{paint}+R_{ice}+1/h} \quad (4)$$

$$\omega_2 = \frac{1}{\sqrt{R_{paint}(R_{ice}+1/h)C_{paint}C_{ice}}}, \quad (5)$$

$$z = \frac{1}{2}\sqrt{R_{paint}\left(R_{ice}+1/h\right)C_{paint}C_{ice}}\;\frac{\left(1+\dfrac{R_{paint}}{\left(R_{ice}+1/h\right)}\right)C_{paint}+C_{ice}}{R_{paint}C_{paint}C_{ice}}, \quad (6)$$

$$K_2 = \frac{1}{R_{paint}+R_{ice}+1/h}, \quad (7)$$

$$\omega_3 = \frac{R_{paint}\left(R_{ice}+1/h\right)C_{ice}}{R_{paint}+R_{ice}+1/h}. \quad (8)$$

The thermal power applied by the paint, denoted P_{elec}, is produced by an electronic dimmer controlled by a voltage $u(t)$ such that:

$$u(s) = \frac{P_{elec}(s)}{G_r}, \quad (9)$$

in which the gain G_r that characterizes the dimmer is defined by

$$G_r = \frac{P_{\max}}{10}. \quad (10)$$

3.2 Parameter Identification

Numerical values of the parameters in relations (1) and (3) were determined using measures recorded at 31 locations on the prototype as shown on figure 5.

To obtain the measures, a pseudo random binary sequence (PRBS) shown in figure 6 (top) was used for the control input $u(t)$.

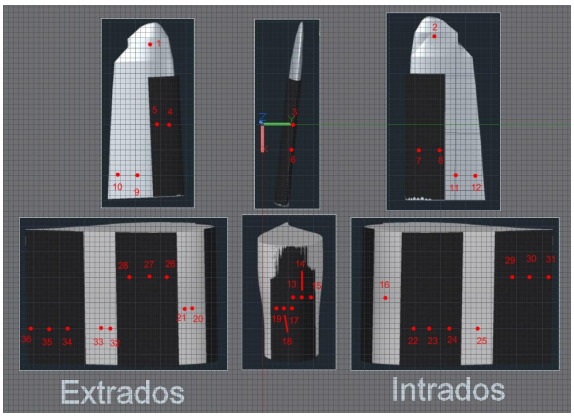

Figure 5: Locations of temperature sensors (red dots) and heating paint strips (black) on the prototype.

This dynamic characterization was repeated for all the thermocouples on the heating strips and for different wind and ice conditions. As an example, the frequency responses of the models obtained for sensor #6 are shown in figures 7 and 8. Similar results were obtained for the other sensors.

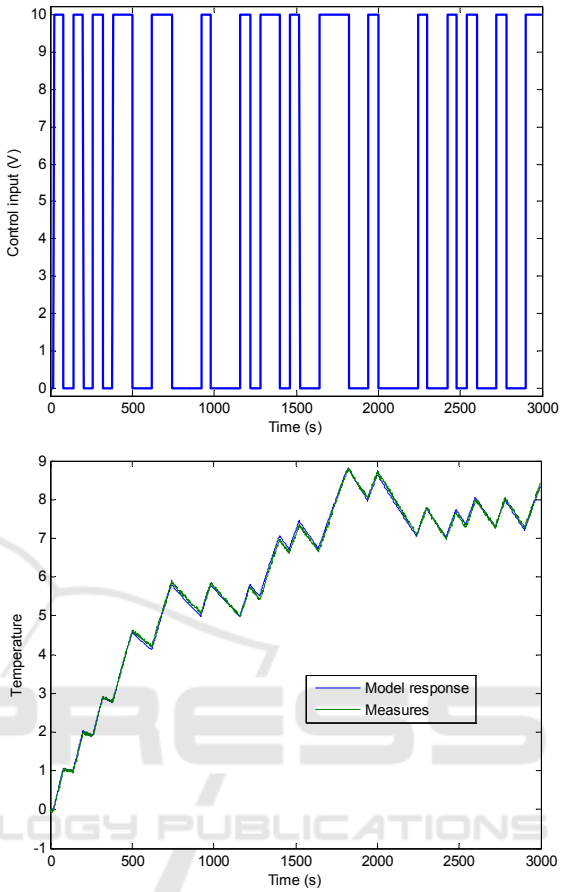

Figure 6: PRBS used for identification and a comparison of the model response with the measured temperature from sensor #6 (readjusted at °0C) with ice (T_{amb} = – 10°C) and without wind.

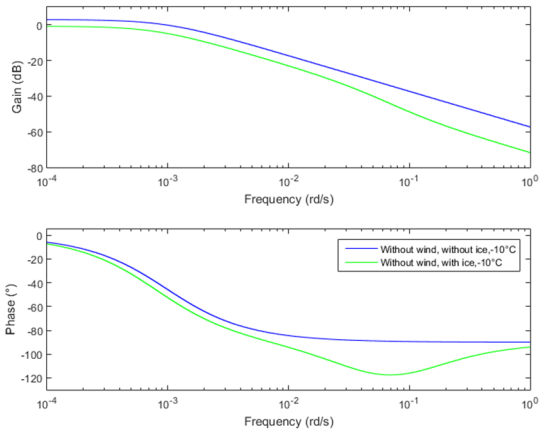

Figure 7: Comparison of the frequency response of the models obtained for sensor #6, without wind (T_{amb} = -10°C) and with or without ice.

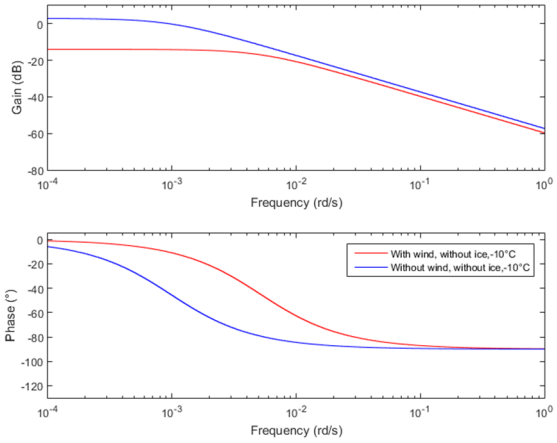

Figure 8: Comparison of the frequency response of the models obtained for sensor #6, without ice (T_{amb} = - 10°C) and with or without wind (25 m/s speed).

Comparisons of the model frequency responses reveal that:

- ice on the blade reduces the static gain and the corner frequency of the frequency responses;
- wind increases the corner frequency of the frequency responses and in accordance with relation (1) reduces the static gain through the variation in the convection exchange coefficient h.

It can be concluded from this comparison that:

- the dynamic behavior variations induced by ice can be exploited to detect ice accretion,
- wind also creates dynamic behavior variations that are linked to the convection exchange coefficient h.

4 ICE DETECTION SOLUTION

The differences in the dynamic behaviors observed with or without ice and highlighted in the previous section were next exploited with an observer to detect ice accretion. The feedback configuration of the observer means that the control signal, which is used to deduce ice accretion, can be immunized against noise and disturbances, while revealing the significant dynamical behavior differences due to ice accretion.

4.1 Observer-based Ice Accretion Detection

The observer-based detection proposed is described in figure 9. To detect ice, a control input $u(t)$ is applied to the dimmer that controls the heating of the paint strips. The resulting signal T_{blade} measured by a temperature sensor is recorded. The same signal $u(t)$ is applied to the model obtained for the same sensor without wind and without ice. The estimated temperature $\hat{T}_{blade}$ thus obtained is compared to T_{blade} to produce an error ε_T. The error is the input of a controller that modifies the input $u(t)$ to force the output of the model to cancel the error ε_T. The higher the output $v(t)$ of the controller, the greater the difference between the model and the blade ice accretion state. Signal $v(t)$ after filtering by filter $F(s)$ can thus be used to decide whether icing occurs or not.

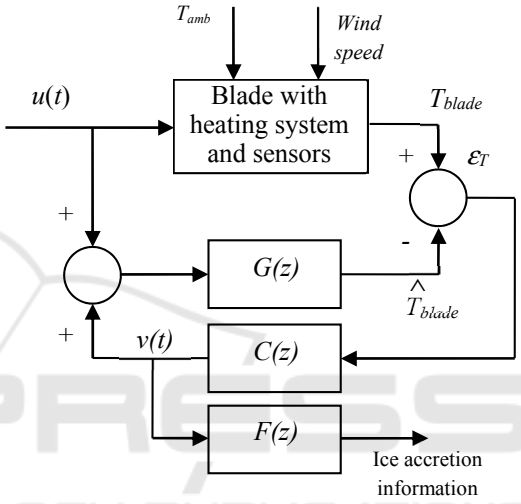

Figure 9: Observer-based ice accretion detection.

4.2 Validation in a Climatic Chamber: without Wind

Let $G_6(s)$ be the transfer function linking the control voltage $u(t)$ to the temperature measured by sensor #6 with

$$G_6(s) = \frac{0.013}{0.0067 + s}. \quad (11)$$

The numerical values of parameters in relation (11) are computed to fit time responses in figure 6 through an optimization program. The Z-transform of $G_4(s)$ with a sampling period of 1s is thus

$$G_6(z^{-1}) = \frac{0.01296}{1 - 0.9933 z^{-1}}. \quad (12)$$

A controller $C(z^{-1})$ was designed to impose a gain crossover frequency at least 10 times greater than the corner frequency of $G_6(z^{-1})$ on the feedback

connection of $G_6(z^{-1})$ and $C(z^{-1})$. This controller is given by:

$$C\left(z^{-1}\right)=\frac{5.2619+0.1045z^{-1}-5.1574z^{-2}}{1-1.3318z^{-1}+0.3318z^{-2}}. \quad (13)$$

The following low pass filter

$$F\left(z^{-1}\right)=\frac{0.00995z^{-1}}{1-0.99z^{-1}}. \quad (14)$$

was then tuned (after a Fourier transform analysis) to attenuate the control input noise. For each test presented in the sequel, temperature was initially regulated at -1°C (initial condition) using the system designed in (Sabatier *et al.*, 2016). A 10V control is sent to the dimmer to use maximum power to engage the melting ice very quickly. The time responses from the sensor (process), the output of the model (estimated temperature) and at the output of the controller $v(t)$ in the cases without or with ice are represented respectively in figure 10 and figure 11.

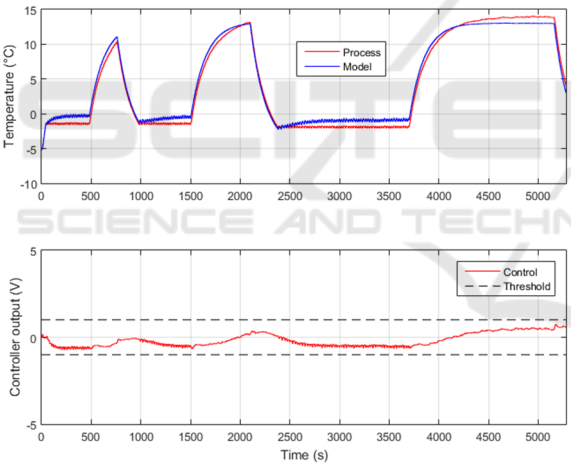

Figure 10: Case without ice: comparison of the temperature measure from sensor #6 (process) and from the corresponding model (top) and control signal $v(t)$ (bottom)

On the ice-free test of figure 10, the blue curve represents the temperature provided by the identified model that links the dimmer control voltage to the temperature measured by sensor #6. This response is very close to the real temperature that is shown in red: the error is less than 10% (less than 2 ° C error for a delta T of 15 ° C). As a result, the control signal $v(t)$ at the output of the controller remains below a threshold fixed at 1V.

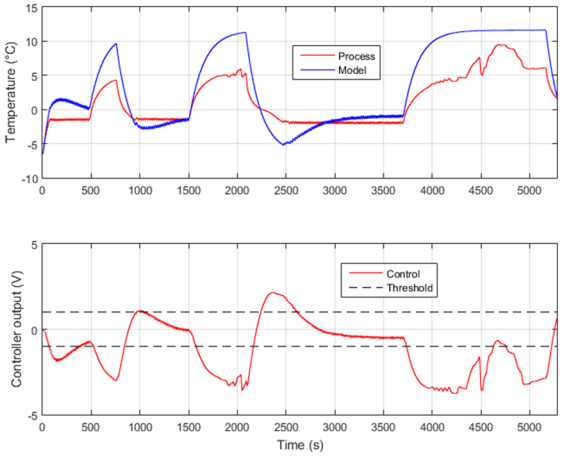

Figure 11: Case with ice: comparison of the temperature measure from sensor #6 (process) and from the corresponding model (top) and control signal $v(t)$ (bottom).

For the test with ice shown in figure 11, a large part of the power produced by the paint is absorbed by the state change in the ice/water and does not cause an increase in temperature. This leads to a small static gain for the system linking the dimmer control voltage and the temperature (thus a mismatch of the model to the system). Therefore a negative correction is produced to force the model to behave like the process. The control signal $v(t)$ at the output of the controller now exceeds the threshold.

The temperature peaks that occur at times [≈2000s] and [4500-5000s] correspond to movements of water and air bubbles in the space between the ice and the plate. This phenomenon confirms that the ice is melting. In conclusion, the detection system of figure 9 produces a control signal whose level becomes large enough to make it possible to detect the presence of ice.

4.3 Validation in a Climatic Chamber: with Wind

With wind, thermal convection needs to be modeled precisely. The convection coefficient of h (in W. °C^{-1}) which appears in figure 4 has to be computed to parameterize the model in figure 9 as a function of the wind, and in particular the corner frequency ω_c defined by relation (2). To define the dependence of ω_c on the wind speed (to correctly detect the ice-free case), a series of characterization tests with a PRBS dimmer control voltage was carried out for winds up to 18 m/s. For each test, a model was identified leading to an estimation of parameter $\tau = 1/\omega_c$.

Variations of the time constant τ with respect to wind speed are shown on figure 12 that highlights the model dependence on the wind speed. This figure also shows the approximation used in the model.

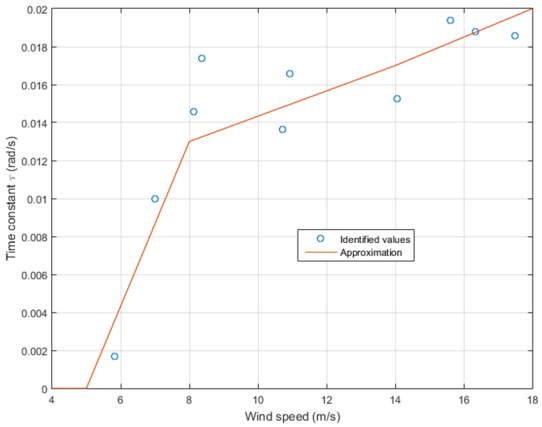

Figure 12: Impact of the wind speed on the parameter $\tau = 1/\omega_c$ and approximation used in the model.

Given the previous analysis, the corner frequency of the model G in figure 9 can be adjusted to take wind conditions (or blade rotation speed) into account. The results obtained with this strategy are shown on figure 13 and 14. In figure 13, in spite of wind conditions and without ice, the control signal $v(t)$ remains small (less than the 1V threshold) thus leading to the conclusion of no ice accretion. Conversely, with ice accretion, figure 14 shows that the control signal $v(t)$ required to force the model to behave like the real process is larger than the 1V threshold. Thus ice accretion can be deduced.

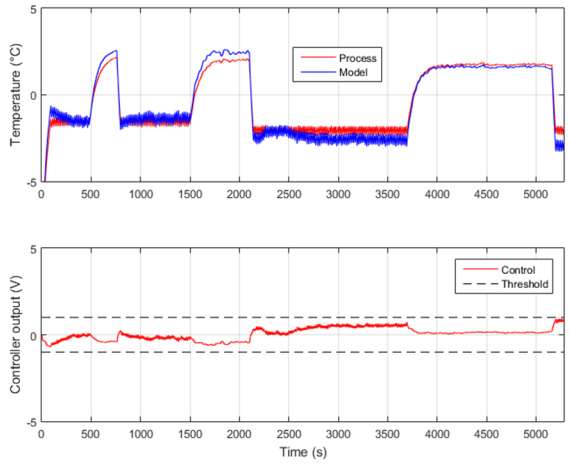

Figure 13: Case without ice and with wind (10 m/s): comparison of the temperature measure from sensor #6 (process) and from the corresponding model (top) and control signal $v(t)$.

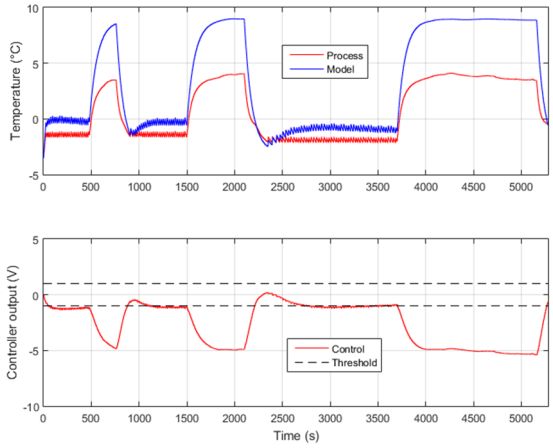

Figure 14: Case with ice and with wind (10 m/s): comparison of the temperature measure from sensor #6 (process) and from the corresponding model (top) and control signal $v(t)$.

These results validate the efficiency of the proposed method, and especially the relevance of using an observer to detect the presence of ice. With ice, the control signal becomes large enough to make a decision.

5 CONCLUSIONS

Using a de-icing device recently proposed by (Sabatier *et al.*, 2016) that involves a conductive polymer paint to heat relevant surfaces of the blade under electrical potential difference, an ice accretion detector is proposed. The differences in the dynamical thermal behavior of the paint with or without ice accretion are exploited with an observer to determine whether icing occurs or not. The proposed strategy was evaluated on a blade prototype in a climatic chamber. These tests showed the efficiency of the method both with and without wind.

REFERENCES

Berbyuk V., Peterson B.; Möller, J., 2014, Towards early ice detection on wind turbine blades using acoustic waves, *SPIE Proceedings*, Vol. 9063.

Botura G., Fisher K., 2003, Development of Ice Protection System for Wind Turbine Applications, *BOREAS VI, FMI, Pyhätunturi, Finland,* p. 16

Dalili N., Edrisy A., Carriveau R., 2009, A review of surface engineering issues critical to wind turbine performance, *Renewable and Sustainable Energy Reviews, Vol. 13*, pp. 428–438.

Frohboese P., Anders A., 2007, Effects of Icing on Wind Turbine Fatigue Loads*, Journal of Physics: Conference Series, Vol. 75.*

Ganander, H., Ronsten, G., 2003, Design load aspects due to ice loading on wind turbine blades. *In Proceedings of the 2003 BOREAS VI Conference. Pyhätunturi, Finland. Finnish Meteorological Institute.*

Hochart, C., Perron J., Fortin G., Ilinca A., 2008, Wind turbine performance under icing conditions, *Wind Energy, Vol. 11, N° 4, pp 319–333.*

Homola M. C., Nicklasson P. J., Sundsbø P. A., 2006, Ice sensors for wind turbines, *Cold Regions Science and Technology Vol. 46, pp 125–131*

Jasinski, W.J., Noe, S.C., Selig, M.S., Bragg, M.B, 1998, Wind turbine performance under icing conditions. *Transactions of the ASME, Journal of solar energy engineering, Vol. 120, pp 60–65.*

Kimura, S., Sato T., Kosugi K., 2003, The Effect of Anti-Icing Paint on the Adhesion Force of Ice Accretion on a Wind Turbine Blade, *BOREAS VI, FMI, Pyhätunturi, Finland, p. 9*

Kraj, A. G., Bibeau E. L., 2010, Phases of icing on wind turbine blades characterized by ice accumulation, *Renewable Energy, Vol. 35, N° 5, pp 966–972*

Laakso, T., Peltola E., 2005, Review on blade heating technology and future prospects, *BOREAS VII, FMI, Saariselkä, Finland, p. 12*

Owusu K. P., Kuhn D. C. S., Bibeau E. L., 2013, Capacitive probe for ice detection and accretion rate measurement: *Proof of concept, Renewable Energy, Vol. 50, pp 196–205*

Parent O., Ilinca A., 2011, Anti-icing and de-icing techniques for wind turbines: *Critical review, Cold Regions Science and Technology, Vol. 65, N° 1, pp 88–96*

Rescoll, 2011, Rescoll Society, web site of the technology owner, http://www.rescoll.fr/nos_technologies_paniplast.php.

Ronsten, G., 2004, Svenska erfarenheter av vindkraft i kallt klimat - nedisning, iskastoch avisning. Elforsk report 04:13.

Sabatier J., Lanusse P., Feytout B., Gracia S., 2016, CRONE control based anti-icing / deicing system for wind turbine blades, *Control Engineering Practice, Vol. 56, pp 200–209*

Seifert H., 2003, Technical requirements for rotor blades operating in cold climate. In Proceedings of the 2003 *BOREAS VI Conference. Pyhätunturi, Finland. Finnish Meteorological Institute.*

Skrimpas G. A., Kleani K., Mijatovic N., Sweeney C. W. Jensen B. B., Holboell J., 2016, Detection of icing on wind turbine blades by means of vibration and power curve analysis, *Wind Energy, Vol. 19, 1819–1832.*

Virk M., Homola M., Nicklasson P., 2010, Effect of Rime Ice Accretion on Aerodynamic Characteristics of Wind Turbine Blade Profiles*, Wind Engineering, Vol. 34, N° 2, pp 207-218.*